Antarct. Meteorite Res., 13, 39–54, 2000

A dark inclusion in the Manych LL (3.1) ordinary chondrite: A product of strong shock metamorphism

Tomoko Kojima, Tomomi Yatagai and Kazushige Tomeoka

Department of Earth and Planetary Sciences, Faculty of Science, Kobe University, Nada, Kobe 657–8501

Abstract: A dark inclusion (MNC-1) from the Manych LL (3.1) chondrite contains elliptical objects ("augen"; 50–500 μm in long axis) embedded in a fine-grained matrix. Most augen are composed of parallel intergrowths of fine laths of Fe-rich olivine, high-Ca pyroxene, and Na-rich feldspathic glass that commonly enclose coarse grains (5–80 μm in diameter) of Fe-rich olivine (Fo_{62-83}). The matrix of MNC-1 consists predominantly of interlocking, granular grains ($<$1–10 μm in diameter) of Fe-rich olivine (Fo_{63-66}), interstitial high-Ca pyroxene and Na-rich feldspathic glass. Both the Manych host and MNC-1 have experienced strong shock metamorphism. The texture and mineralogy of MNC-1 suggest that the matrix of MNC-1 experienced shock melting, whereas the "augen" represent unmelted precursor material. Bulk major element composition of MNC-1 is generally similar to the average values for LL chondrites, except that MNC-1 is considerably depleted in S and enriched in FeO. The large S depletion may be due to volatilization during impact-induced melting. Texture and mineralogy of the augen are distinct from those of the Manych host, so MNC-1 may not be a melt dike which formed *in situ* in the host rock. MNC-1 appears to be a xenolith that solidified elsewhere on the LL chondrite parent body and was later incorporated to the present location.

1. Introduction

Some ordinary chondrites contain dark-colored xenoliths that may be related to carbonaceous chondrites (*e.g.*, Wasson and Wetherill, 1979). Although some of the xenoliths appear to represent CM-like material (Wasson and Wetherill, 1979), the rest have not been clearly classified. Most of the unclassified xenoliths are described to consist mainly of fine-grained Fe-rich olivine (*e.g.*, Kurat, 1970; Fodor and Keil, 1976; Noonan *et al.*, 1976; Zolensky *et al.*, 1993; Semenenko and Girich, 1999), thus appear to be rather similar to C3 chondrites.

Dark lithic clasts that chemically and mineralogically resemble C3 chondrites commonly occur in CV and CR chondrites, and are called dark inclusions (DIs) (*e.g.*, Fruland *et al.*, 1978; Johnson *et al.*, 1990; Endress *et al.*, 1994; Buchanan *et al.*, 1997). DIs are composed largely of fine-grained Fe-rich olivine. Originally, DIs were interpreted as aggregates of nebular dusts (Bischoff *et al.*, 1988; Kurat *et al.*, 1989; Palme *et al.*, 1989) or as fine-grained impact breccia (Bischoff *et al.*, 1993). However, recent studies revealed abundant evidence that DIs are products of

aqueous alteration and subsequent thermal metamorphism on the meteorite parent body. It was suggested that the fine-grained Fe-rich olivine in DIs resulted from dehydration of phyllosilicates during thermal metamorphism (Kojima *et al.*, 1993; Krot *et al.*, 1995; Kojima and Tomeoka, 1996). This has been supported by more recent studies (Buchanan *et al.*, 1997; Krot *et al.*, 1997, 1998a, b, 1999).

In this paper we present the results of detailed mineralogical and petrographic study of a dark inclusion in the Manych LL (3.1) chondrite. The inclusion, hereafter termed MNC-1, has been briefly described by Zolensky *et al.* (1993). The present results revealed that MNC-1 is distinct from DIs in CV3 chondrites. The texture and mineralogy suggest that MNC-1 experienced a complex sequence of alteration and metamorphism, including strong shock-induced melting, probably on the meteorite parent body.

2. Sample and methods

We used a polished thin section (#4787-2; $\sim$1.7 cm^2 total area) of the Manych LL (3.1) chondrite, provided by the American Museum of Natural History. It was examined with an optical microscope, a scanning electron microscope (SEM; JEOL JSM-5800) and an electron microprobe analyzer (EPMA; JEOL JXA-8900). The SEM is equipped with an Oxford ISIS energy-dispersive X-ray spectrometer (EDS) microanalysis system. EDS analyses were obtained at 15 kV and 0.4 nA, with a focused electron beam of $\sim$2 μm in diameter. Corrections were made by the Phi-Rho-Z method. EPMA analyses of silicates were obtained at 15 kV and 12 nA with a focused electron beam of $\sim$2 μm in diameter, and matrix effects were corrected by Bence and Albee procedures. As standards for quantitative SEM-EDS and EPMA analyses, well-characterized natural and synthetic minerals were used. Analytical totals for Na-rich glass are generally low (96–98 wt%), probably due to Na-loss during measurement.

Bulk major element composition of MNC-1 was determined by the EPMA defocused electron beam (100 μm in diameter) technique. All elements were analyzed as oxides; weight percents of FeO, FeS and metallic Fe were calculated from the obtained data as follows. 1) All S was regarded to be present as FeS, of which amount can be estimated from the obtained SO_3 content. 2) Metallic Fe was calculated from the modal abundance of Fe-Ni metal. 3) FeO content was calculated by subtraction of Fe sited in FeS and Fe-Ni metal from the analyzed total FeO concentration.

3. Results

3.1. Petrography of MNC-1

MNC-1 is approximately 1.8$\times$3.5 mm^2 in size. It might have been originally larger because it was artificially cut at one end. In transmitted light, it is distinctly darker than the host and contains many brownish translucent to transparent elliptical objects (50–500 μm in long axis) embedded in almost opaque matrix (Fig.

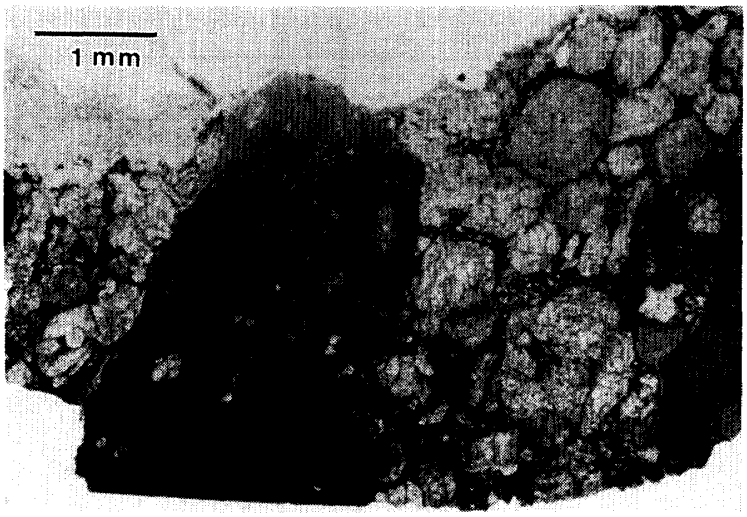

Fig. 1. An optical photomicrograph of a portion containing MNC-1. In plane polarlized light. MNC-1 contains elliptical "augen" and their fragments that are embedded in an opaque matrix. Note that most of the augen and chondrules in the host are elongated in approximately NE-SW direction in this photo.

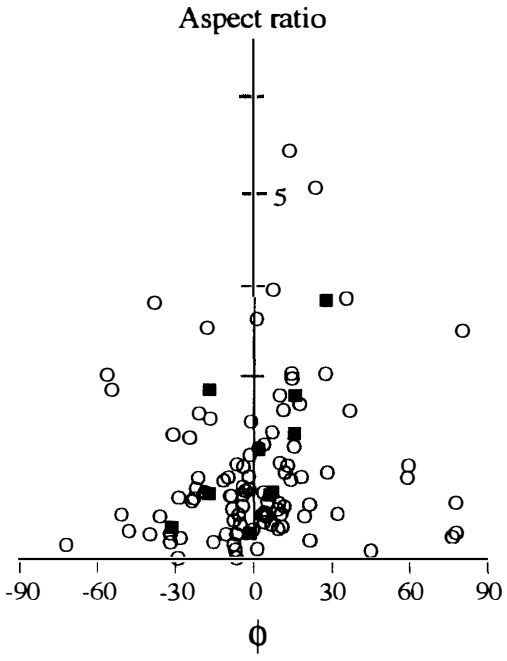

Fig. 2. Plot of aspect ratio vs. direction of long axis (ϕ) of augen and chondrules in the Manych host. The average direction of long axis is fixed to be $\phi=0$. ○: Chondrules in the Manych host. ■: Augen in MNC-1.

1). The elliptical objects probably correspond to the "augen" ("eyes" in German) described by Zolensky *et al.*, (1993). Aspect ratios of the augen vary from 1.4 to 3.8 (Fig. 2). Long axes of the augen are roughly parallel to each other. Along with the augen, angular to subangular objects (5–100 μm in long dimension) are also abundantly included in MNC-1; they are mineralogically and texturally identical to the augen. They are probably fragments of augen.

The augen consist mainly of olivine (Fo_{62-83}), high-Ca pyroxene (En_{52-60} Wo_{17-32}), Na-rich feldspathic glass (4–11wt% Na_2O) and minor Fe-Ni metal ($Fe_{96-95}Ni_{5-4}$) (Tables 1, 2). Volume proportions of the constituents and textures differ considerably between augen; three textural types are recognized. The most

Table 1. Selected electron microprobe analyses of oxide phases in MNC-1 (wt%).

	1	2	3	4	5	6	7	8	9
	Ol	Ol	Ol	Ol	Ol	Cpx	Cpx	Gl	Gl
SiO_2	39.1	37.0	38.0	36.3	36.5	50.6	52.1	68.9	64.8
Al_2O_3	0.05	<0.03	0.08	0.10	0.04	0.69	1.33	19.9	18.1
TiO_2	0.06	<0.03	<0.03	0.03	0.03	0.17	0.04	0.04	0.04
FeO	17.5	29.4	22.4	32.1	31.2	14.1	12.3	0.73	0.93
MnO	0.16	0.42	0.46	0.57	0.56	0.48	0.49	<0.03	<0.03
MgO	43.3	33.0	38.3	30.2	30.5	21.6	20.1	0.32	0.43
CaO	0.05	0.11	0.05	0.09	<0.03	8.40	12.0	0.40	0.86
Na_2O	<0.03	<0.03	<0.03	<0.03	<0.03	1.53	1.27	5.17	10.5
K_2O	<0.03	<0.03	<0.03	<0.03	<0.03	0.18	0.22	0.74	0.73
Cr_2O_3	0.11	0.06	<0.03	0.25	0.18	0.29	0.41	0.04	<0.03
NiO	<0.03	<0.03	0.05	0.04	0.30	<0.03	<0.03	<0.03	<0.03
Total	100.3	100.0	99.3	99.7	99.3	98.0	100.3	96.2	96.4
Si	5.95	5.99	5.98	5.98	6.00	7.68	7.72	9.17	8.83
Al	0.01		0.01	0.02	0.01	0.12	0.23	3.13	2.90
Ti	0.01			0.00	0.00	0.02	0.00	0.00	0.00
Fe	2.22	3.97	2.95	4.43	4.29	1.79	1.52	0.08	0.10
Mn	0.02	0.06	0.06	0.08	0.08	0.06	0.06		
Mg	9.82	7.97	8.98	7.42	7.49	4.89	4.43	0.06	0.09
Ca	0.01	0.02	0.01	0.02		1.37	1.90	0.06	0.12
Na						0.45	0.36	1.33	2.78
K						0.03	0.04	0.13	0.13
Cr	0.01	0.01		0.03	0.02	0.04	0.05	0.00	0.00
Ni			0.01	0.01	0.04				
Fo	81.6	66.8	75.3	62.6	63.6				
En						60.7	56.4		
Wo						17.0	24.2		

Ol=olivine, Cpx=Ca-pyroxene, Gl=glass. Atomic ratios are calculated as O=24.
Data 1, 2 and 8 from auge#9 (type II), 3 from auge#29 (type I), 4, 5 and 9 from matrix, 6 from auge#20 (type III), 7 from auge#27 (type I).

Table 2. Selected electron microprobe analyses of opaque phases in MNC-1 (wt%).

#	1	2	3	4	5
	Kam	Kam	Tae	Tae	Tro
Si	<0.03	<0.03	<0.03	<0.03	<0.03
Cr	0.03	<0.03	<0.03	0.14	0.03
Mn	<0.03	<0.03	<0.03	<0.03	<0.03
Fe	93.8	94.7	46.3	62.1	63.6
Co	1.43	1.29	0.31	0.33	0.05
Ni	4.68	4.45	53.2	36.9	0.10
P	<0.03	<0.03	<0.03	<0.03	<0.03
S	<0.03	<0.03	<0.03	<0.03	36.3
Total	99.9	100.4	99.8	99.5	100.1

Kam=kamacite, Tae=taenite, Tro=troilite.
# 1 coexists with 3, 2 coexists with 4 and 5.

common type (type I) consists largely of parallel intergrowths of fine laths ($<1\,\mu$m in width, <1–$10\,\mu$m in length) of olivine, pyroxene and glass (Figs. 3a, b). In some augen, directions of the parallel intergrowths differ from portion to portion (Fig. 3c). Coarse olivine grains (5–80 μm in diameter), some with Fe-Mg zoning (Fo_{76-83} in cores to Fo_{62-63} in rims) are commonly embedded in the fine intergrowths; the fine, parallel laths bend along the surfaces of the coarse olivine grains, exhibiting a flow-like texture (Fig. 3b). Grains of Fe-Ni metal of various sizes (<1–$50\,\mu$m in

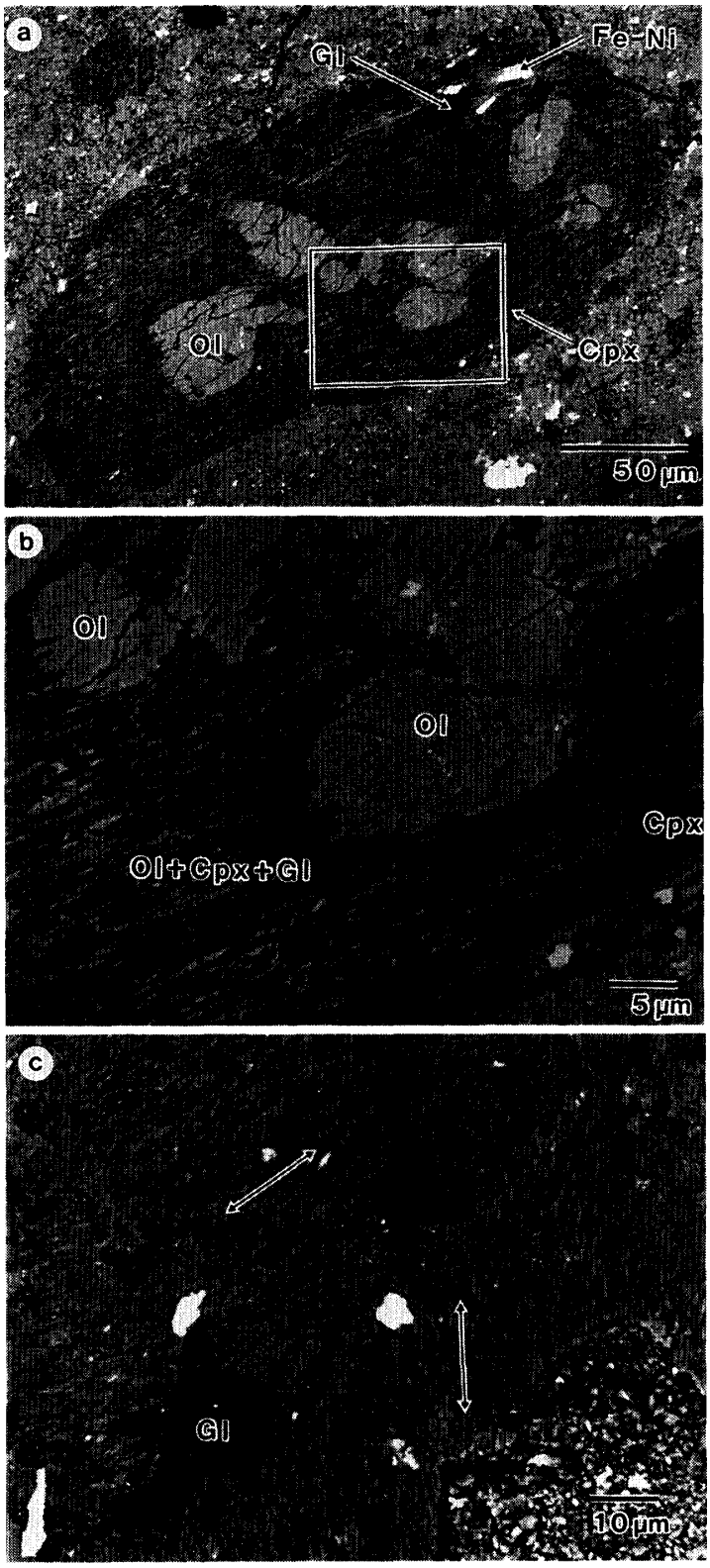

Fig. 3. Backscattered electron (BSE) images showing various textures of augen.

(a) A type I auge composed of Fe-rich olivine (Ol), high-Ca pyroxene (Cpx), Na-rich feldspathic glass (Gl) and Fe-Ni metal.

(b) An enlarged image of the boxed area in (a). Most part of the auge consists of parallel intergrowths of Fe-rich olivine (light gray), high-Ca pyroxene (dark gray) and glass (almost black). The parallel intergrowths bend along the surfaces of coarse olivine grains.

(c) An internal portion of a type I auge. In upper left portion, the intergrowths are parallel to NE-SW direction of the photo, while they are parallel to N-S direction in lower right portion. The porous portion in the lower right corner is a hollow which might have formed during sample preparation by falling off of a mineral grain.

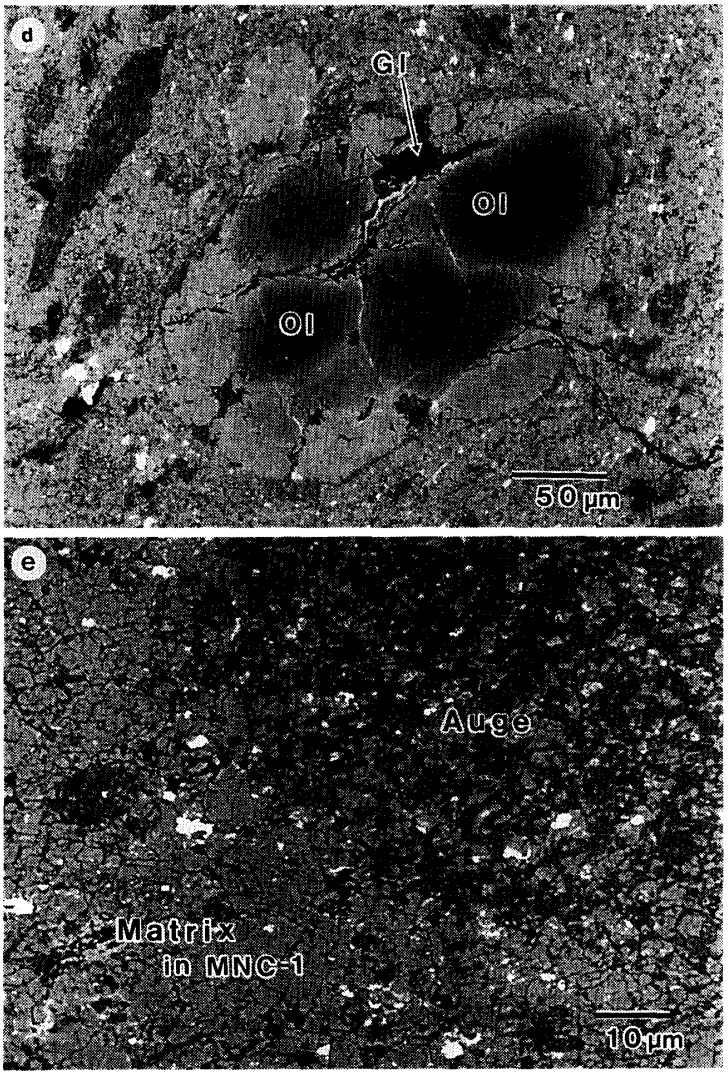

Fig. 3. (continued).
(d) A type II auge composed of coarse-grained olivine and minor glass. The olivine grains show Fe-Mg zoning.

(e) A boundary between a type III auge (upper right) and matrix. The auge consists of finegrained olivine (light gray) and high-Ca pyroxene (dark gray), and intergrades with the matrix.

diameter) also occur in the intergrowths. Type II augen are aggregates of coarse olivine grains (10–100 μm in diameter) with minor amounts of interstitial high-Ca pyroxene, glass and Fe-Ni metal, being similar to porphyritic olivine chondrules (Fig. 3d). The olivine grains commonly show Fe-Mg zoning, like those in type I augen. A major difference between type I and II augen is that the latter do not contain the parallel intergrowths. Type III augen consist exclusively of fine-scale ($<10\,\mu$m, mostly $<5\,\mu$m in diameter) intergrowths of olivine and high-Ca pyroxene (Fig. 3e). Olivine generally occurs as equigranular grains, while pyroxene occurs as elongated fine laths ($\sim1\,\mu$m in width and $\sim5\,\mu$m in length). Particles of Fe-Ni metal also occur. Augen of this type intergrade with the matrix in MNC-1 (Fig. 3e).

Matrix of MNC-1 consists predominantly of interlocking granular grains (<1–$10\,\mu$m in diameter) of Fe-rich olivine (Fig. 4a). The olivine is homogeneous (Fo_{63-66}) and compositionally identical to the olivine in augen that shows no Fe-Mg zoning (Table 1). Narrow interstices between the olivine grains are generally filled with laths or anhedral grains of high-Ca pyroxene (Fig. 4a). Na-rich feldspathic

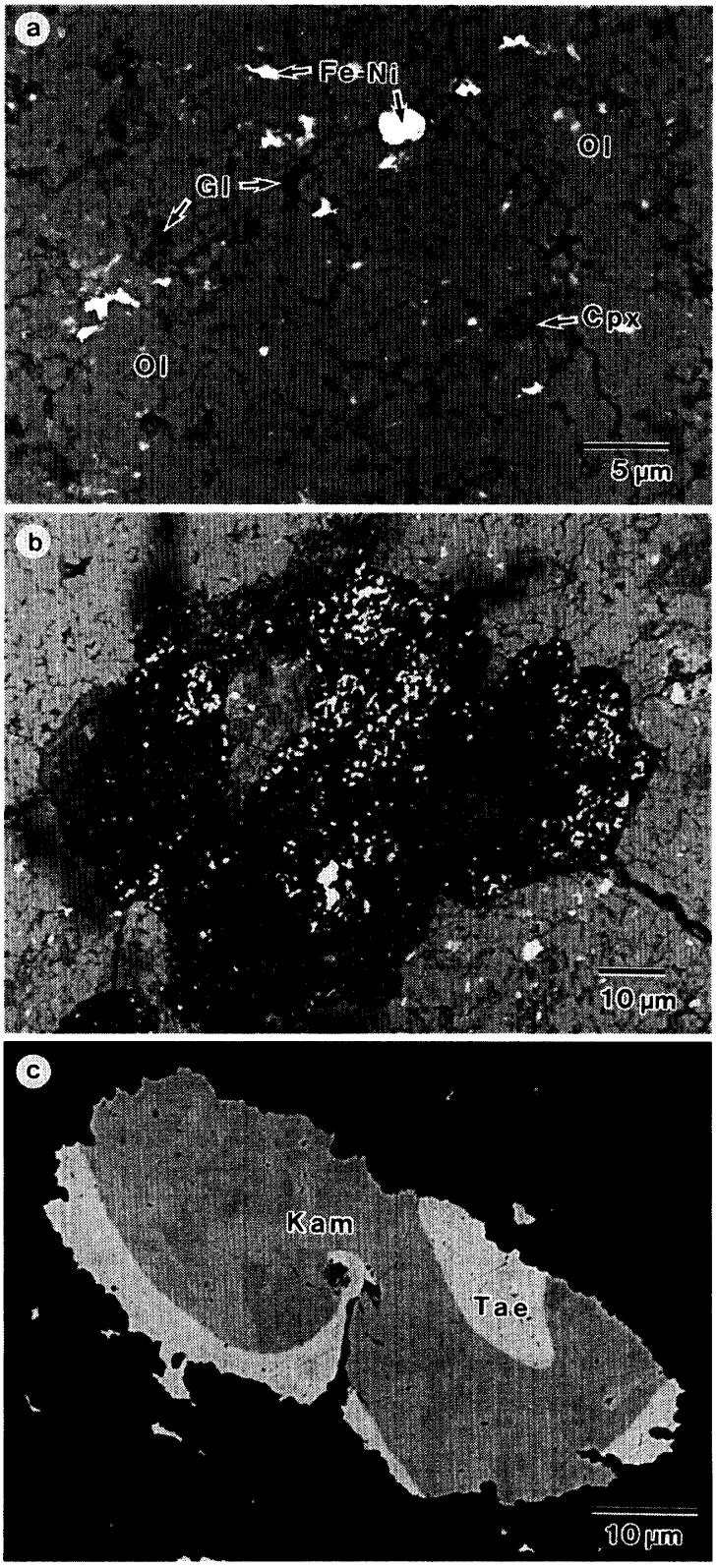

Fig. 4.

(a) A high-magnification BSE image of the matrix. Abbreviations are the same as in Fig. 3.

(b) A portion in the matrix that is dominated by Na-rich feldspathic glass. Numerous tiny inclusions of Fe-Ni metal (white spots) and a clast composed of olivine and high-Ca pyroxene are embedded in the glass.

(c) An Fe-Ni metal grain in the matrix. It consists of well-separated kamacite (Kam) and taenite (Tae). Note that the outline of the grain shows many notches, suggesting that metal in the peripheral portions has melted and intruded into interstices between olivine grains.

glass also commonly occurs in minor amounts. A relatively large volume of Al-, Na-rich glass ($\sim 100 \times 100\,\mu m^2$ in area) was found in a portion in the matrix (Fig. 4b). Fe-Ni metal grains of various sizes (< 1–$80\,\mu m$ in diameter) are abundantly dispersed throughout the matrix. Most of the relatively large ($> 10\,\mu m$ in diameter) grains are slightly elongated in the same direction as augen. They commonly consist of well-separated kamacite ($Fe_{92-93}Ni_{5-4}$) and taenite ($Fe_{47-63}Ni_{53-37}$) (Fig. 4c); the kamacite contains variable amounts of Co, Cr and Mn (Table 2). In contrast to the Manych host, troilite is extremely rare in MNC-1; only one grain ($20\,\mu m$ in diameter) was found to coexist with kamacite and taenite.

The bulk major element composition of MNC-1 is shown in Table 3.

Table 3. Bulk major element composition of MNC-1 (wt%).

	*MNC-1	Manych	LL average	CV3 average
SiO_2	39.0 (0.73)	39.7	40.6	34.0
Al_2O_3	2.43 (0.53)	2.34	2.24	3.22
TiO_2	0.10 (0.03)	0.12	0.13	0.16
FeO	22.7#	14.6	17.4	26.8
MnO	0.45 (0.03)	0.33	0.35	0.19
MgO	27.6 (0.92)	24.6	25.2	24.6
CaO	1.96 (0.41)	1.90	1.92	2.62
Na_2O	1.22 (0.28)	0.83	0.95	0.49
K_2O	0.16 (0.05)	0.12	0.10	0.05
Cr_2O_3	0.57 (0.06)	0.57	0.54	0.50
P_2O_5	0.18 (0.12)	0.20	0.22	0.25
Ni	0.93 (0.28)	0.99	1.07	1.40
FeS	0.08#	8.39	5.79	4.05
Fe (met)	2.90#	4.11	2.44	0.16
Total	100.3	98.8	99.0	98.5
Fe (total)	20.4	20.6	19.6	23.6

Data of Manych, average LL and CV3 chondrites are from Jarosewich (1990).
* Average of 92 analyses. Standard deviations are also shown in parentheses.
# Calculated from the analyzed oxide wt. %. For the detail, see the text in the section Sample and Method.

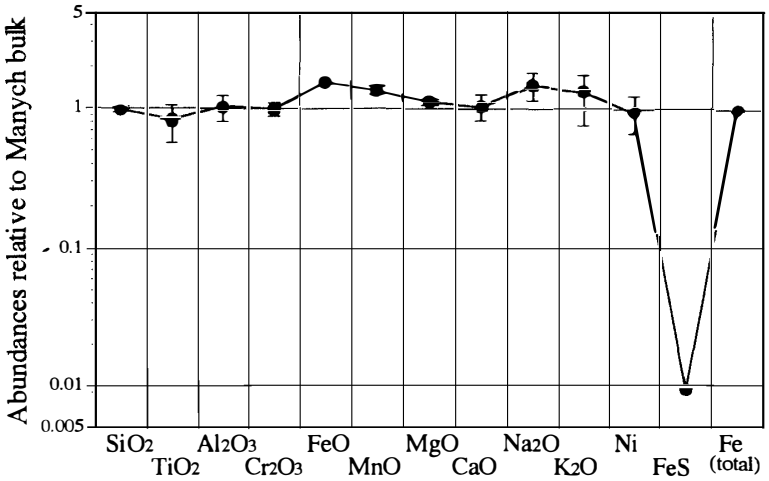

Fig. 5. Bulk major element abundances of MNC-1, relative to the Manych host. Data of Manych from Jarosewich (1990). The bars represent 1σ of analyses.

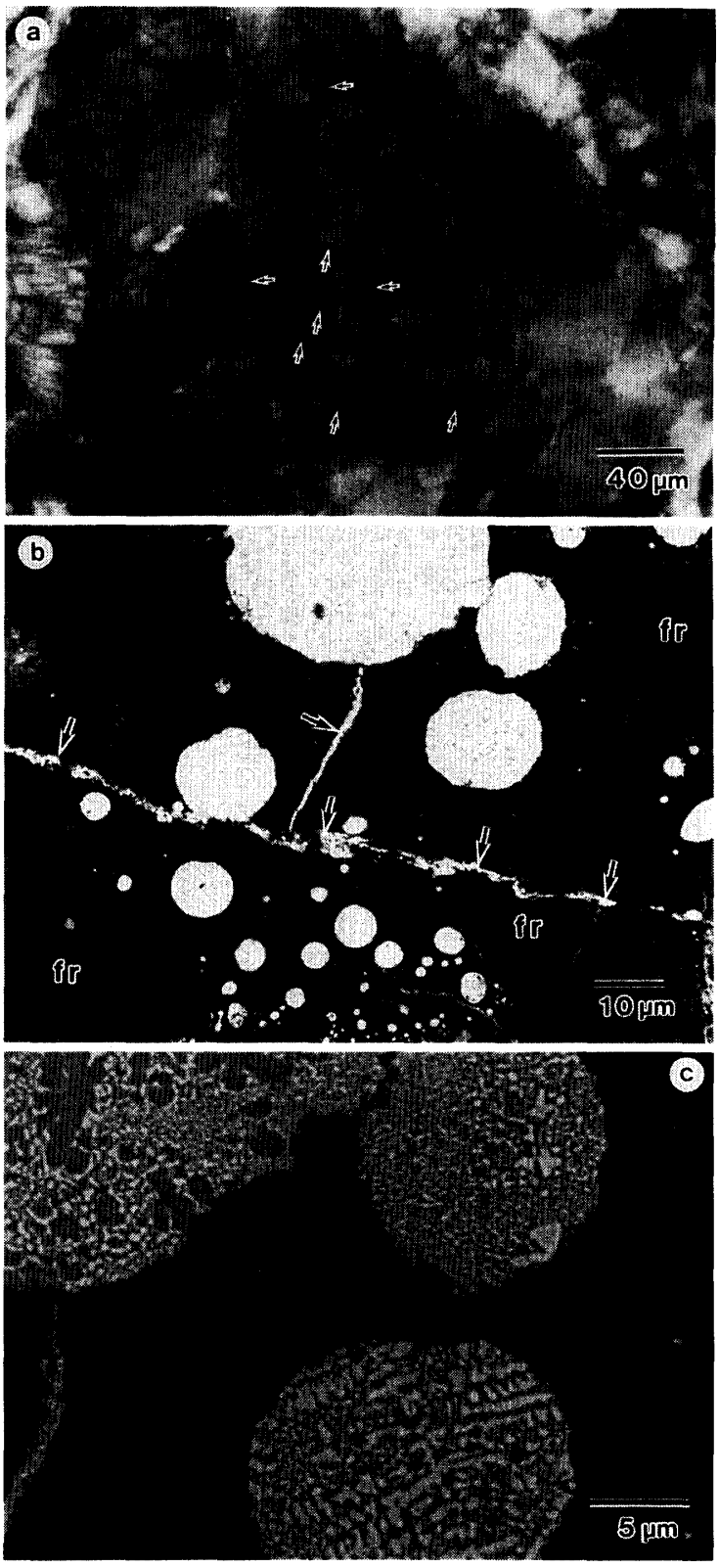

Fig. 6. Shock features in the Manych host (a–c) and in MNC-1 (d, e).

(a) An olivine grain with planar fractures parallel to two different orientation (arrows). This olivine also shows mosaicism. In crossed polarized light.

(b) A BSE image of a portion in a melt pocket. Sub-round silicate fragments (fr) and Fe-Ni metal/troilite globules of various size are embedded in a glassy groundmass. Veins of Fe-Ni metal/troilite crosscut the fragments, Fe-Ni metal/troilite globules and groundmass (arrows).

(c) An enlarged image of opaque globules shown in the upper portion in (b). The globules consist of Fe-Ni metal (white) and troilite (light gray) that show dendritic textures.

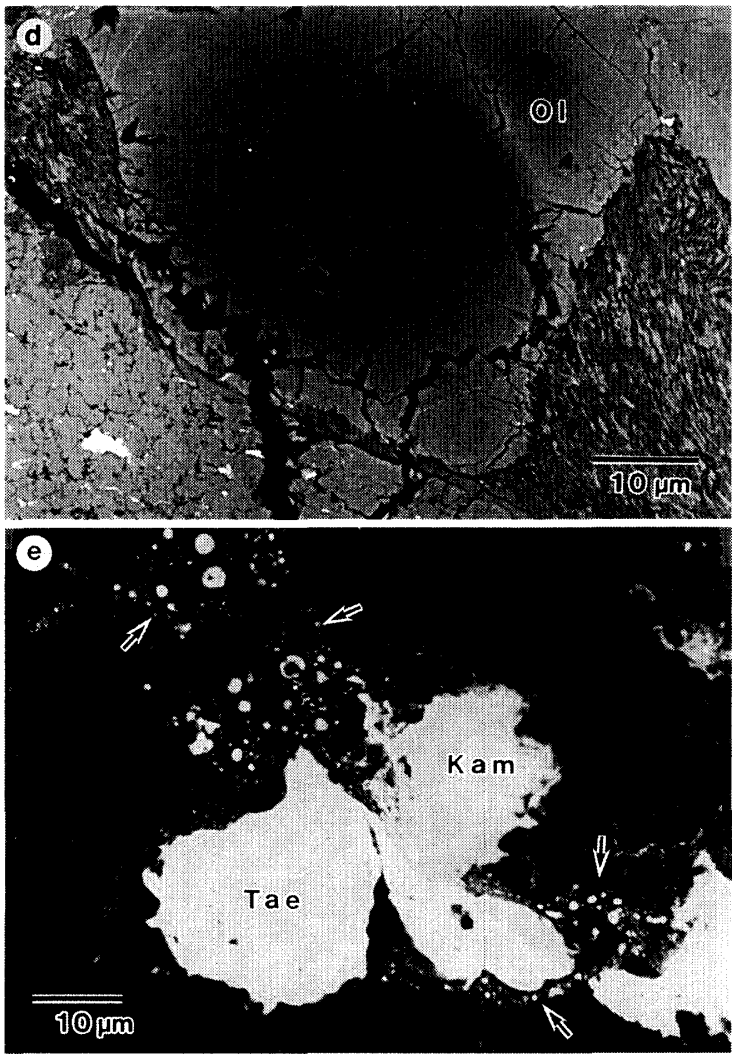

Fig. 6. (continued).

(d) A BSE image of an olivine grain in a type I auge. The grain shows three parallel sets of planar fractures. Triangular pits at the intersecting points of the fractures probably formed during sample preparation. This grain also shows strong Fe-Mg zoning.

(e) Fe-Ni metal grains in the matrix. Peripheral portions of the grains (arrows) contain numerous tiny globules that resemble those shown in (b) and (c).

Compared with the Manych host, MNC-1 is considerably depleted in S (Table 3, Fig. 5). In contrast, it is enriched in Mn, Na, K and FeO. Despite the high FeO concentration, total atomic Fe content is comparable to the value for the Manych host (Table 3, Fig. 5). Contents of other major elements are comparable to those of Manych. Except for the large S depletion and high FeO concentration, MNC-1 is similar in bulk composition to LL chondrites.

3.2. Shock features in the host Manych and MNC-1

The present study revealed abundant evidence suggesting that the Manych host meteorite experienced strong shock metamorphism. Chondrules and opaque nodules are apparently flattened in the same direction (Figs. 1, 2). In crossed polarized light, coarse olivine grains in chondrules commonly show undulatory extinction and mosaicism (Fig. 6a). Parallel sets of planar fractures are also common in olivine and low-Ca pyroxene grains; some grains show two or more intersecting parallel sets (Fig. 6a). Interchondrule matrix is highly compacted. Corrigan *et al.* (1997) reported that the porosity of matrix of Manych is 1%.

Another remarkable shock indicator is the abundant occurrence of melt pockets and veins. The melt commonly occurs along chondrule-matrix and opaque nodule-matrix boundaries, and its volume reaches up to $600 \times 200\,\mu m^2$ in area. It consists of numerous opaque globules (<1–$40\,\mu m$ in diameter) and subrounded silicate fragments set in an aphanitic groundmass (Fig. 6b). Compositions of the groundmass varies widely, and are generally rich in Na, Al and Si. The opaque globules in the melt commonly consist of Fe-Ni metal and troilite, and exhibit dendritic texture (Fig. 6c). Thin veins ($<2\,\mu m$ in thickness) of metal and/or troilite occur in some of the melt pockets; they are usually connected to opaque globules and crosscut both the groundmass and silicate fragments (Fig. 6b). Based on the criteria of Stöffler *et al.* (1991), these features suggest that Manych was shocked to stage S4 or above.

MNC-1 was apparently also affected by shock metamorphism. Coarse olivine grains in type I and II augen commonly show undulatory extinction, mosaicism and parallel sets of planar fractures (Fig. 6d). Some olivine grains in matrix, probably derived from fragmented augen, might have recrystallized in the solid state like those described by Stöffler *et al.* (1991), because they appear to be single crystals with pale yellow color in plane polarized light, but show fine-grained polycrystalline texture in crossed polarized light. Fe-Ni metal in the matrix appears to have partly melted and intruded into interstices between olivine grains (Fig. 4c); in places, it forms tiny globules similar to those in the melts in the host (Fig. 6e). The glass-rich area in matrix (Fig. 4b) contains a silicate fragment and tiny particles of Fe-Ni metal, and looks like a melt pocket.

3.3. Textures at the boundary between MNC-1 and the host

At the boundary between MNC-1 and the host rock, some characteristic textures are observed. In some portions of the boundary, a high density of large cracks occurs. In other areas, narrow ($\sim 15\,\mu m$ in width), discontinuous bands composed of extremely fine-grained material occur between MNC-1 and the host (Fig. 7a); the grains are hardly discernible by the SEM. Based on the composition, the fine-grained material consist mainly of Fe-rich olivine (approximately Fo_{63}). Tiny subrounded grains of Fe-rich olivine, low-Ca and high-Ca pyroxenes are embedded in the fine-grained material. Parts of chondrules in the host just adjacent to the boundary are considerably fragmented. Melt pockets and shock veins are particularly abundant in the peripheries of MNC-1; some of the veins occur in the fine-grained bands. A significant volume of melt ($500 \times 300\,\mu m^2$ in area) occurs in a portion at the boundary (Fig. 7b). The melt encloses many chondrule fragments and appears to have originated mainly from the host Manych material. A part of the melt intrudes into MNC-1, through the boundaries of olivine grains in matrix of MNC-1 (Fig. 7c).

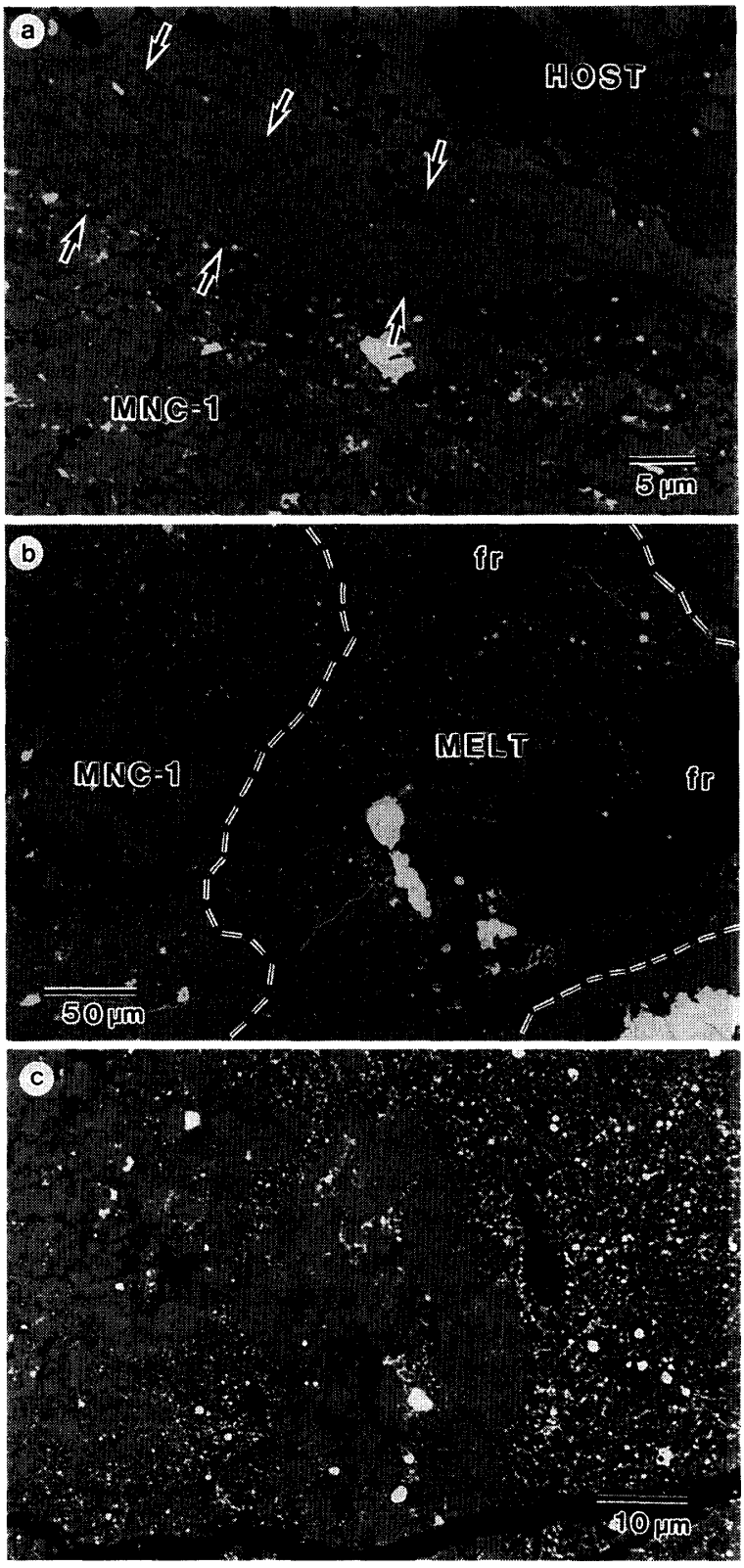

Fig. 7.

(a) A boundary between MNC-1 (lower left) and the Manych host (upper right). A discontinuous, narrow band composed of extremely fine-grained materials occurs between MNC-1 and the host (arrows).

(b) A melt pocket at a boundary between MNC-1 (left) and the Manych host (upper and lower left). Outlines of the melt pocket are indicated by broken lines. The melt contains subrounded fragments of various size (fr) that derived from chondrules in the host.

(c) An enlargement of the upper central portion in (b). The melt with tiny particles of Fe-Ni metal apparently intrudes into MNC-1 (left) through grain boundaries.

4. Discussion

4.1. Origin of MNC-1

The present results revealed that MNC-1 is quite different in texture and mineralogy from DIs in CV3 chondrites. Fe-rich olivines in DIs occur as loosely packed, fibrous to lath-like grains (*e.g.*, Kojima *et al.*, 1993; Kojima and Tomeoka, 1996; Krot *et al.*, 1997). On the other hand, Fe-rich olivine in MNC-1 occurs mainly as interlocking granular grains (Fig. 4a). The texture and mineralogy of MNC-1, *i.e.*, interlocking granular olivine with interstitial high-Ca pyroxene, Na-rich feldspathic glass and Fe-Ni metal, suggest that MNC-1 experienced igneous melting processes due to shock metamorphism.

Recent studies revealed that significant volumes of melt have been produced by shock metamorphism of chondritic materials of relatively low petrologic types. Yamaguchi *et al.* (1999) studied the Ramsdorf L chondrite and found an almost entirely melted portion that might have been originally petrologic type 3 or 4. The melted matrix of the portion consists of Fe-rich olivine, high-Ca pyroxene and Na-rich feldspathic glass, being similar in mineralogy to the matrix of MNC-1. Ruzicka *et al.* (1998) reported that the Julesberg L3 chondrite contains a large shock-melt region (<2.5 cm in diameter) as well as many igneous-textured inclusions. Of particular interest is that one of the inclusions (Jl-7) closely resembles MNC-1; Jl-7 contains angular-to-rounded clasts, some apparently broken chondrules, set in a fine-grained groundmass rich in olivine and feldspathic glass (Fig. 2e in Ruzicka *et al.*, 1998). The authors interpreted that Jl-7 formed as a clast-laden shock melt. A melt rock fragment has been reported also from the Adzhi-Bogdo chondrite, which is an LL3-6 chondritic breccia (Bischoff *et al.*, 1993).

The similarities between MNC-1 and the melt objects in other ordinary chondrites suggest that MNC-1 formed as a shock-induced melt. The augen in MNC-1 are probably partly melted and ablated clasts derived from a precursor rock; type II augen (Fig. 3d) are apparently broken porphyritic chondrules. Coarse olivine grains in the augen have Mg-rich cores (Figs. 3d, 6d), suggesting that the precursor is an unequilibrated chondrite. Type III augen (Fig. 3e) resemble some clasts in the inclusion Jl-7 from Julesberg (Ruzicka *et al.*, 1998), and appear to be debris almost completely assimilated into the melt. The most common type I augen show a characteristic texture composed of fine-scale parallel intergrowths of olivine, high-Ca pyroxene and Na-rich feldspathic glass (Figs. 3a–c); to our knowledge, such a texture has not been reported from any other chondritic material. Probably, type I augen originate from chondrules which have experienced a complex sequence of alteration and deformation processes. The processes may include oxidization, which is responsible for the higher FeO content in MNC-1 than in common LL chondrites (Table 3). However, details of the alteration sequence are currently unknown.

4.2. Relationships between MNC-1 and the Manych host

From the bulk major element composition (Table 3), it seems plausible that the precursor of MNC-1 was an LL chondritic material. The large depletion of S in MNC-1 (Table 3, Fig. 5), as well as in Jl-7 (Ruzicka *et al.*, 1998), may be due to vaporization during the melting. On the other hand, some observations conflict with that MNC-1 is a melt dike that formed *in situ*. Augen probably represent a remnant precursor rock, and their texture and mineralogy are distinct from those of the Manych host: low-Ca pyroxene is absent in MNC-1, while they are abundant in chondrules in Manych (Dodd, 1978), and fine-scale parallel intergrowths in the type I augen (Figs. 3a–c) are not observed in any component of the host. In addition, MNC-1 is significantly more oxidized than the Manych host (Table 3, Fig. 5). Thus, we suggest that MNC-1 is a xenolith that solidified elsewhere and was later incorporated to the present location.

MNC-1 is distinct in texture and mineralogy from melt veins and pockets that occur in the Manych host, probably due to different precursor material. Different cooling rates may be responsible for the difference, too. Fe-Ni metal grains in MNC-1 consist of well-separated kamacite and taenite (Fig. 4c, Table 2), indicating that they were cooled at a relatively slow rate; if cooling was rapid, they would show dendritic textures similar to those described by Scott (1982), or would have averaged, homogeneous compositions (Smith and Goldstein, 1977). In contrast, cooling rates of the melts in the host were apparently rapid, because the melts are glassy to aphanitic (Fig. 6b) and opaque nodules in them show dendritic textures (Fig. 6c). The difference is consistent with that MNC-1 is a xenolith that formed at a different location.

Some melt pockets in the Manych host are crosscut by thin veins of Fe-Ni metal and/or troilite (Fig. 6b). Formation of such a feature would require at least two shock events; silicate melts with immiscible metal and troilite formed during an impact event, and, after the melt had solidified, veins formed by injection of preferentially melted metal and troilite into fractures. Similar features have been reported from strongly shocked ordinary and carbonaceous chondrites (Stöffler *et al.*, 1991; Scott *et al.*, 1992). Therefore, Manych probably has experienced multiple shock events. A relatively large melt pocket occurs at the boundary between MNC-1 and the host, and the melt intrudes to MNC-1 (Figs. 7b, c). The texture suggests that formation of the melt, *i.e.*, one of the shock events which Manych experienced, postdates incorporation of MNC-1 to the present location. MNC-1, which certainly had solidified then, should have been affected by the later shock event(s). The glass-rich area in matrix (Fig. 4a) may be a melt pocket that formed by local melting that occurred after solidification of MNC-1. Probably, Fe-Ni metal grains in MNC-1, along with some part of silicates, also partly melted during the later shock event(s) (Figs. 4c, 6e).

4.3. Formation of the Manych LL3 breccia

Chondrite regolith or fragmental breccias generally consist of submm- to cm-sized clasts and xenoliths embedded in a fine-grained clastic matrix that appar-

ently derived from the same rock as the clasts (*e.g.*, Bischoff *et al.*, 1993). The Manych host is an agglomerate of chondrules and their fragments that are individually surrounded by matrix (Fig. 1), and does not look like a regolith or fragmental breccia. However, most of the chondrules in Manych are more or less rounded fragments of larger objects (Dodd, 1978), suggesting that the Manych components certainly have experienced considerable fragmentation and ablation. MNC-1 might have been produced during such a process.

Based on our observations, we propose a possible model to explain the present texture in Manych. The process probably occurred on an incompletely consolidated, heterogeneous planetesimal. During an impact event, individual chondrules that had been loosely stuck to each other fell apart and were partly fragmented, then reaccumulated on the planetesimal along with the matrix material. MNC-1, *i.e.* a fragment of a solidified melt which had been produced elsewhere by a former shock event, was incorporated at that time. Shock metamorphism subsequently occurred to result in chondrule flattening (Figs. 1, 2) and formation of melt veins and pockets (Figs. 6b, c, e, 7b, c).

Acknowledgments

We thank Drs. M. E. Zolensky, M. K. Weisberg and M. Prinz for providing the polished thin section. We also thank Dr. A. Lin for valuable discussion and information. The manuscript was benefited by helpful reviews by Drs. A. Bischoff and A. N. Krot. The EPMA analysis was carried out at the Venture-Business Laboratory, Kobe University.

References

Bischoff, A., Palme, H., Spettel, B., Clayton, R. N. and Mayeda, T. K. (1988): The chemical composition of dark inclusions from the Allende meteorite. Lunar and Planetary Science XIX. Houston, Lunar Planet. Inst., 88–89.

Bischoff, A., Geiger, T., Palme, H., Spettel, B., Schultz, L., Scherer, P., Schlüter, J. and Lkhamsuren, J. (1993): Mineralogy, chemistry, and noble gas contents of Adzhi-Bogdo—an LL3-6 chondritic breccia with L-chondritic and granitoidal clasts. Meteoritics, **28**, 570–578.

Buchanan, P. C., Zolensky, M. E. and Reid, A. M. (1997): Petrology of Allende dark inclusions. Geochim. Cosmochim. Acta, **61**, 1733–1743.

Corrigan, C. M., Zolensky, M. E., Dahl, J., Long, M., Weir, J., Sapp, C. and Burkett, P. J. (1997): The porosity and permeability of chondritic meteorites and interplanetary dust particles. Meteorit. Planet. Sci., **32**, 509–515.

Dodd, R. T. (1978): The composition and origin of large microporphyritic chondrules in the Manych (L-3) chondrite. Earth Panet. Sci. Lett., **39**, 52–66.

Endress, M., Keil, K., Bischoff, A., Spettel, B., Clayton, R. N. and Mayeda, T. K. (1994): Origin of dark clasts in the Acfer 059/El Djouf 001 CR2 chondrite. Meteoritics, **28**, 26–40.

Fodor, R. V. and Keil, K. (1976): Carbonaceous and noncarbonaceous lithic fragments in the Plainview, Texas, chondrite: Origin and history. Geochim. Cosmochim. Acta, **40**, 177–189.

Fruland, R. M., King, E. A. and McKay, D. S. (1978): Allende dark inclusions. Proc. Lunar Planet. Sci. Conf., 9th, 1305–1329.

Jarosewich, E. (1990): Chemical analyses of meteorites: A compilation of stony and iron meteorite analyses. Meteoritics, **25**, 323–337.

Johnson, C. A., Prinz, M., Weisberg, M. K., Clayton, R. N. and Mayeda, T. K. (1990): Dark inclusions in Allende, Leoville, and Vigarano: Evidence for nebular oxidation of CV3 constituents. Geochim. Cosmochim. Acta, **54**, 819–830.

Kojima, T. and Tomeoka, K. (1996): Indicators of aqueous alteration and thermal metamorphism on the CV parent body: Microtextures of a dark inclusion from Allende. Geochim. Cosmochim. Acta, **60**, 2651–2666.

Kojima, T., Tomeoka, K. and Takeda, H. (1993): Unusual dark clasts in the Vigarano CV3 carbonaceous chondrite: Record of parent body process. Meteoritics, **28**, 649–658.

Krot, A., Scott, E. R. D. and Zolensky, M. E. (1995): Mineralogical and chemical modification of components in CV3 chondrites: Nebular or asteroidal processing? Meteoritics, **30**, 748–775.

Krot, A., Scott, E. R. D. and Zolensky, M. E. (1997): Origin of fayalitic rims and lath-shapes matrix olivine in the CV3 chondrite Allende and its dark inclusions. Meteorit. Planet. Sci., **32**, 31–49.

Krot, A. N., Petaev, M. I., Zolensky, M. E., Keil, K., Scott, E. R. D. and Nakamura, K. (1998a): Secondary Ca-Fe-rich minerals in the Bali-like and Allende-like oxidized CV3 chondrites and Allende dark inclusions. Meteorit. Planet. Sci., **33**, 623–645.

Krot, A. N., Petaev, M. I., Scott, E. R. D., Choi, B.-G., Zolensky, M. E. and Keil, K. (1998b): Progressive alteration in CV3 chondrites: More evidence for asteroidal alteration. Meteorit. Planet. Sci., **33**, 1065–1085.

Krot, A. N., Brearley, A. J., Ulyanov, A. A., Biryukov, V. V., Swindle, T. D., Keil, K., Mittlefehldt, D. W., Scott, E. R. D., Clayton, R. N. and Mayeda, T. K. (1999): Mineralogy, petrology, bulk chemical, iodine-xenon, and oxygen-isotopic compositions of dark inclusions in the reduced CV3 chondrite Efremovka. Meteorit. Planet. Sci., **34**, 67–89.

Kurat, G. (1970): Zur Genese des kohligen Materials im Meteoriten von Tieschitz. Earth Panet. Sci. Lett., **7**, 317–324.

Kurat, G., Palme, H., Brandstätter, F. and Huth, J. (1989): Allende xenolith AF: Undisturbed record of condensation and aggregation of matter in the Solar Nebula. Z. Naturforsch., **44a**, 988–1004.

Noonan, A. F., Nelen, J. and Fredriksson, K. (1976): Mineralogy and chemistry of xenoliths in the Weston chondrite-ordinary and carbonaceous. Meteoritics, **11**, 344–346.

Palme, H., Kurat, G., Spettel, B. and Burghele, A. (1989): Chemical composition of an unusual xenolith of the Allende meteorite. Z. Naturforsch., **44a**, 1005–1014.

Scott, E. R. D. (1982): Origin of rapidly solidified metal-troilite grains in chondrites and iron meteorites. Geochim. Cosmochim. Acta, **46**, 813–823.

Scott, E. R. D., Keil, K. and Stöffler, D. (1992): Shock metamorphism of carbonaceous chondrites. Geochim. Cosmochim. Acta, **56**, 4281–4293.

Semenenko, V. P. and Girich, A. L. (1999): Chondrule embryos or dusty spherules in the Krymka (LL3) chondrite. Meteorit. Planet. Sci., **34**, A106.

Smith, B. A. and Goldstein, J. I. (1977): The metallic microstructures and thermal histories of severely reheated chondrites. Geochim. Cosmochim. Acta, **41**, 1061–1072.

Stöffler, D., Keil, K. and Scott, E. R. D. (1991): Shock metamorphism of ordinary chondrites. Geochim. Cosmochim. Acta, **55**, 3845–3867.

Ruzicka, A., Snyder, G. A. and Taylor, L. A. (1998): Mega-chondrules and large, igneous textured clasts in Julesberg (L3) and other ordinary chondrites: Vapor-fractionation, shock-melting, and chondrule formation. Geochim. Cosmochim. Acta, **62**, 1419–1442.

Wasson, J. T. and Wetherill, G. W. (1979): Dynamical, chemical and isotope evidence regarding the formation locations of asteroids and meteorites. Asteroids, ed. by T. Gehrels. Tucson, Univ. Arizona Press, 926–974.

Yamaguchi, A., Scott, E. R. D. and Keil, K. (1999): Origin of a unique impact-melt rock-the L-chondrite Ramsdorf. Meteorit. Planet. Sci., **34**, 49–59.

Zolensky, M. E., Weisberg, M. K., Barret, R. A. and Prinz, M. (1993): Mineralogy of dark clasts in primitive vs differentiated meteorites. Lunar and Planetary Science XXIV. Houston, Lunar Planet. Inst., 1583–1584.

(Received September 20, 1999; Revised manuscript received January 19, 2000)